Applied Catalysis B: Environmental 211 (2017) 258–265

Contents lists available at ScienceDirect

Applied Catalysis B: Environmental

journal homepage: www.elsevier.com/locate/apcatb

Doping strategy to promote the charge separation in $BiVO_4$ photoanodes

Bo Zhang [a], Haipeng Zhang [a], Zeyan Wang [a,*], Xiaoyang Zhang [a], Xiaoyan Qin [a], Ying Dai [b], Yuanyuan Liu [a], Peng Wang [a], Yingjie Li [c], Baibiao Huang [a,*]

[a] State Key Laboratory of Crystal Materials, Shandong University, Jinan, 250100, PR China
[b] School of Physics, Shandong University, 250100, PR China
[c] School of Energy and Power Engineering, Shandong University, Jinan, 250061, PR China

ARTICLE INFO

Article history:
Received 21 January 2017
Received in revised form 25 March 2017
Accepted 31 March 2017
Available online 2 April 2017

Keywords:
PEC water splitting
$Mo:BiVO_4/Co:BiVO_4$
Charge separation

ABSTRACT

We fabricated $Mo:BiVO_4/Co:BiVO_4$ photoanodes by depositing $Co:BiVO_4$ layers on top of $Mo:BiVO_4$ layers, and demonstrated the enhanced PEC performances with improved charge separation both in the bulk and at the interface by doping strategy in this work. $Co:BiVO_4$ layers in $Mo:BiVO_4/Co:BiVO_4$ photoanodes were found to be important for the enhanced charge separation efficiencies. The surface exposed Co^{2+} ions in $Co:BiVO_4$ layers can act as reactive sites for water oxidation to promote the interfacial charge separation. While, the Co^{2+} doping inside $Co:BiVO_4$ cannot only tune the built in electric fields in $Mo:BiVO_4/Co:BiVO_4$ homojunctions, but also be able to optimize the charge transport in $Co:BiVO_4$ layers to facilitate the bulk charge separation. By optimizing the Co contents and the number of $Co:BiVO_4$ layers in $Mo:BiVO_4/Co:BiVO_4$ photoanodes, 3Mo-1Co-6% consisted of 3 layers of 3% $Mo:BiVO_4$ and 1 layer 6% $Co:BiVO_4$ yields the highest photocurrent of 2.09 mA/cm^2 at 1.23 V vs RHE, with a η_b and η_i value of 77.8% and 86.5%, respectively. This work provides a new thread for the design and fabrication of photoanode with high charge separation efficiencies by doping strategy, which could be helpful for the further improvement of PEC water splitting performances.

1. Introduction

Photoelectrochemical (PEC) water splitting has attracted great interests as potential strategy for hydrogen and oxygen evolution from water by utilizing solar energy, which is expected to be one of the most promising methods to solve energy and environmental issues for human beings [1,2]. In the past few decades, great efforts have been made with the purpose to improve the solar to hydrogen (STH) conversion efficiencies to facilitate the practical applications of PEC water splitting. Up to now, various photoelectrodes have been developed, such as TiO_2, ZnO, $BiVO_4$, α-Fe_2O_3, TaON, Ta_3N_5, etc [3–8]. Among these materials, monoclinic scheelite $BiVO_4$ is regarded as one of the most attractive candidates to fabricate photoanodes due to its suitable band gap of ~2.4 eV and excellent stability against photocorrosions, which is expected to have a high theoretical STH conversion efficiency of ~9.1% under AM 1.5G irradiation [9–11]. However, limited by the poor electrical conductivity, short carrier diffusion length and slow water oxidation kinetics, $BiVO_4$ photoanodes usually suffer from poor charge separation both in the bulk and at the interface during PEC water splitting, which is regarded as the main issue that limits the PEC performance of $BiVO_4$ photoanodes.

In order to improve the charge separation in $BiVO_4$ photoanodes, various methods have been developed, such as coupling $BiVO_4$ with other semiconductors to construct type II heterojunctions to promote the bulk charge separation, and loading oxygen evolution catalysts (OECs), e.g., Co-Pi, CoO_x, FeOOH, NiOOH, to accelerate the surface water oxidation kinetics and facilitate the charge injection at the electrode/electrolyte interface [12–17]. Although, the PEC performances have been effectively improved with the assistance of the above methods with enhanced charge separation efficiency both in the bulk and at the interface. The construction of heterojunctions or loading OECs in $BiVO_4$ photoanodes would inevitably introduce some interfaces, which would generate defects act as carrier traps and recombination centers during PEC water splitting, thus, increase the charge recombination. From this aspect, the fabrication of $BiVO_4$ photoanodes with high charge separation efficiency and reduced charge recombination with fewer defects

* Corresponding authors.
E-mail addresses: wangzeyan@sdu.edu.cn (Z. Wang), bbhuang@sdu.edu.cn (B. Huang).

http://dx.doi.org/10.1016/j.apcatb.2017.03.078
0926-3373/

would be advantageous for the further improvement on their PEC performances.

Doping is a commonly used strategy to tune the electrical properties of semiconductor materials, which has been widely used to improve the electrical conductivity of $BiVO_4$ by doping electron donor ions, such as Mo^{6+} or W^{6+} [18–20]. Beside the effects on improving the electrical conductivity and carrier density in semiconductors, the Fermi levels in semiconductors can also be easily tuned by varying the dopant types and concentrations. For example, the Fermi level is shifted towards the conduction band minimum (CBM) and valence band maximum (VBM) with increasing the concentration of n-type and p-type dopants, respectively [21]. Therefore, if we deposit a layer of $BiVO_4$ doped with electron accepto ions (e.g., Co^{2+} doped $BiVO_4$) on top of $BiVO_4$ layers doped with electron donor ions (e.g., Mo^{6+} doped $BiVO_4$), a built-in electric field would be formed due to the different Fermi levels in donor and acceptor ions doped $BiVO_4$, which would promote the charge separation in the electrodes. On the other hand, as the catalytic activity of cobalt containing OECs typically involves the Co^{2+}/Co^{3+} and Co^{3+}/Co^{4+} redox couples [22–26]. The presence of Co ions on the surface of the electrode could also be similar as cobalt containing OECs, which can act as active centers for water oxidation and promote the interfacial charge separation [27]. More importantly, the absence of any OECs and the perfect lattice matching between Mo:$BiVO_4$ and Co:$BiVO_4$ can greatly reduce the defect numbers in the electrode, which could minimize the charge recombination during PEC water splitting. As a result, the charge separation efficiencies both in the bulk and at the interface are expected to be improved in Mo:$BiVO_4$/Co:$BiVO_4$ photoanodes with enhanced PEC performances even without the assistance of OECs, which has not been reported yet to the best of our knowledge.

In order to demonstrate the above concept, we fabricated Mo:$BiVO_4$/Co:$BiVO_4$ photoanodes and investigated their PEC performances in this work. As expected, the PEC performances of Mo:$BiVO_4$/Co:$BiVO_4$ photoanodes were greatly enhanced without the loading of any OECs, which were attributed to the improved charge separation both in the bulk and at the interface. Co:$BiVO_4$ layers were found to be important for the enhanced charge separation efficiencies, which can not only act as reactive sites for water oxidation to promote the interfacial charge separation, but also be able to tune the built in electric fields and the charge transfer in Co:$BiVO_4$ layers to improve the bulk charge separation in Mo:$BiVO_4$/Co:$BiVO_4$ photoanodes. The effects of Co doping concentrations and the number of Co:$BiVO_4$ layers on the PEC performances of Mo:$BiVO_4$/Co:$BiVO_4$ photoanodes were also systematically investigated and optimized in this work.

2. Results and discussions

As illustrated in Fig. 1, Mo:$BiVO_4$/Co:$BiVO_4$ homojunction photoanodes were fabricated by a simple spin coating method following subsequent annealing processes (see details in Experimental Section.). Two layers of Mo:$BiVO_4$ were firstly deposited on FTO substrates with Mo doping concentration of 3% according to the reported value optimized for PEC water splitting [28,29]. Then, two layers of Co:$BiVO_4$ were deposited on Mo:$BiVO_4$ layers following the same procedure to fabricate Mo:$BiVO_4$/Co:$BiVO_4$ photoanodes. In order to optimize the PEC performances, Mo:$BiVO_4$/Co:$BiVO_4$ with different Co doping concentrations, namely, 0%, 2%, 4%, 6% and 8%, respectively, were also fabricated, which were denoted as aMo-bCo-c%, where a and b is the layer numbers of Mo:$BiVO_4$ and Co:$BiVO_4$ ($a+b=4$), respectively, and c% ($c=0, 2, 4, 6, 8$) is the Co con-tents in Co:$BiVO_4$ layers. For comparison, pristine $BiVO_4$, 3% Mo:$BiVO_4$ and 6% Co:$BiVO_4$ were also fabricated.

There structures and morphologies of as prepared samples were characterized by X-ray diffraction (XRD) and scanning electron microscopy (SEM). As shown in Fig. S1, all these samples are pure phase of monoclinic $BiVO_4$ without the appearance of any other impurities, which indicate the Mo or Co doping did not induce the formation of any secondary phases. Fig. S2 shows the SEM images of pristine $BiVO_4$, 3% Mo:$BiVO_4$, 6% Mo:$BiVO_4$ and 2Mo-2Co-6%. As can be seen in this figure, all samples are consisted of some small nanoparticles with irregular shapes. However, the mean sizes of these nanoparticles are quite different from each other. The diameters of the nanoparticles in $BiVO_4$, 3% Mo:$BiVO_4$, 6% Co:$BiVO_4$ and 2Mo-2Co-6% are 150–200, 80–100, 150–200, and 80–150 nm, respectively. And the cross-sectional SEM images shown in the insets of Fig. S2 indicate all the samples have the similar thicknesses of ~200 nm. The transmitance and absorption spectra of the above samples were also measured by UV–vis spectrometer equipped with integrated spheres as shown in Fig. S3. All the samples exhibit similar absorption spectra with absorption edges around 500 nm. And the band gap of $BiVO_4$, 3% Mo:$BiVO_4$, 6% Co:$BiVO_4$ and 2Mo-2Co-6% is estimated to be 2.40, 2.38, 2.35 and 2.39 eV, respectively, which indicate the Mo or Co doping did not change the band gap of $BiVO_4$ notably.

In order to probe the valence states of the dopant ions, e.g., Mo or Co ions, in the as-prepared Mo:$BiVO_4$/Co:$BiVO_4$ photoanodes, X-ray photoelectron spectroscopy (XPS) measurements were also performed. As shown in Fig. S4a, two characteristic peaks located at 232.2 and 235.4 eV arising from Mo 3d 5/2 and 3d 3/2 signals can be observed in 3% Mo:$BiVO_4$, which is accordant with that of prior reports on Mo:$BiVO_4$ and suggest Mo ions are mainly present as Mo^{6+} to substitute V atoms in $BiVO_4$ [30,31]. The XPS peaks at 780.0 and 795.2 eV can be assigned to Co 2p 3/2 and 2p 1/2 peaks, respectively, which is quite similar as the reported values of CoO (Fig. S4b) [32,33]. This indicate that Co could be existed as Co^{2+} in Co:$BiVO_4$. Comparing the pristine $BiVO_4$, the Bi 4f and V 2p XPS peaks of both 3% Mo:$BiVO_4$ and 6% Co:$BiVO_4$ shifted to higher binding energies as shown in Fig. S4c and d, which could be due to the interactions of dopant ions, e.g., Mo^{6+} and Co^{2+}, with Bi and V atoms. And this could also confirmed that Mo^{6+} and Co^{2+} have been doped into $BiVO_4$ lattice. In order to identify the substitution position of Co^{2+} in Co:$BiVO_4$, the formation energy (E_f) were calculated by means of periodic density functional calculations within GGA + U approach. And the E_f of Co_{Bi} and Co_V is calculated to be 3.70 and 6.94, respectively, which indicates Co^{2+} would substitute Bi^{3+} in $BiVO_4$ as electron acceptors. The concentration of Co and Mo dopants in as prepared samples were also measured by XPS. And the measured Mo concentration in 3% Mo:$BiVO_4$ is 5.24%. And the Co concentration in 2%, 4%, 6%, 8% Co:$BiVO_4$ samples is measured to be 2.7, 5, 7.5, 9.3%, respectively. The slightly higher content of both Mo and Co atoms measured by XPS could be due to the surface segregation of the dopant ions, which is accordant with the results reported by Luo et al. [34].

As Mo^{6+} and Co^{2+} substitutes V^{5+} and Bi^{3+} in Mo:$BiVO_4$ and Co:$BiVO_4$, respectively, the doping of Mo^{6+} and Co^{2+} in $BiVO_4$ would be expected to introduce energy levels near the bottom of the CB and the top of the VB in the forbiden band of $BiVO_4$ as donor and acceptor levels, respectively. To confirm this assumption, the band structures of $BiVO_4$, 3% Mo:$BiVO_4$ and 6% Co:$BiVO_4$ were calculated as shown in Fig. S5. As expected, the donor and acceptor levels by Mo^{6+} and Co^{2+} doping can be observed in Mo:$BiVO_4$ and Co:$BiVO_4$, respectively, which lie at the bottom of the CB and near the top of the VB of $BiVO_4$, respectively. Therefore, Mo^{6+} doping is expected to have little effect on the width of the band gap of $BiVO_4$, and Co^{2+} doping could slightly narrowed the band gap of $BiVO_4$, which is accordance with the observations on the light absorption spectra of Mo:$BiVO_4$ and Co:$BiVO_4$ as shown in Fig. S3.

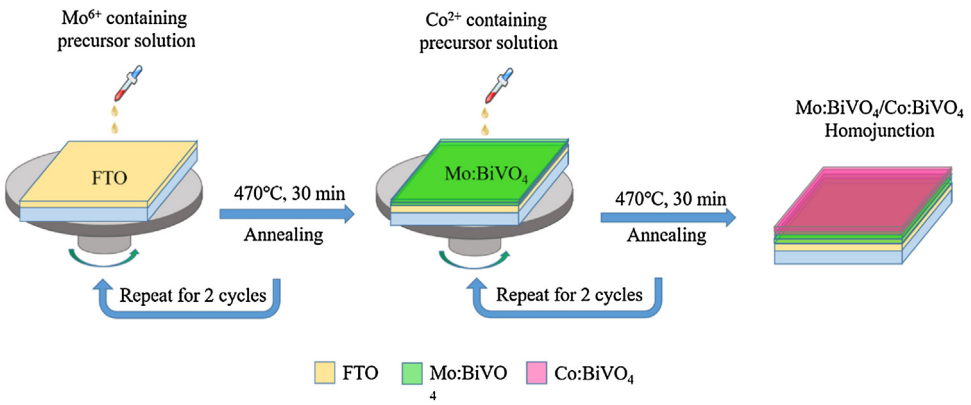

Fig. 1. Schematic diagram to illustrate the fabrication procedure of $Mo:BiVO_4/Co:BiVO_4$ photoanodes.

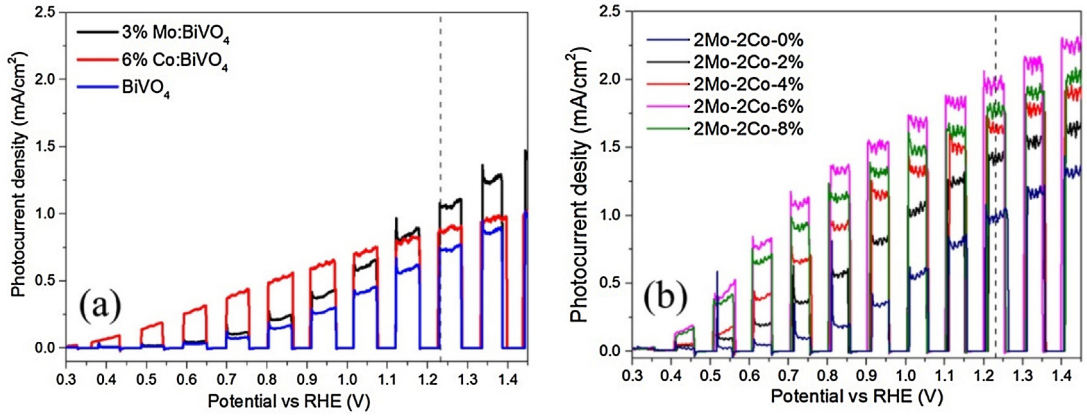

Fig. 2. Photocurrent density versus applied potential curves (J-V) of (a) $BiVO_4$, 3% $Mo:BiVO_4$ and 6% $Co:BiVO_4$ photoanodes, and (b) $Mo:BiVO_4/Co:BiVO_4$ photoanodes with different Co doping concentrations with a scan rate of 10 mV/s under irradiation of chopped AM 1.5G simulated solar light (100 mW/cm^2) in 0.1 M potassium phosphate electrolyte solution (pH = 7).

The PEC measurements were performed by using a three electrode configuration with as prepared samples as the working electrode, a Pt sheet as the counter electrode and saturated calomel electrode (SCE) as the reference electrode measured in 0.1 M potassium phosphate electrolyte (pH = 7) under chopped AM 1.5 G simulated solar light (100 mW/cm^2). The J-V curves of $BiVO_4$, 3% $Mo:BiVO_4$ and 6% $Co:BiVO_4$ were firstly measured. As shown in Fig. 2a, the photocurrents of $BiVO_4$ and 3% $Mo:BiVO_4$ increase slowly with the increase of applied bias with an onset potential of ~0.5 V vs RHE and yield a photocurrent density of 0.45 and 0.93 mA/cm^2 at 1.23 V vs RHE, respectively, which are comparable with the reported values [10]. Different from $BiVO_4$ and $Mo:BiVO_4$, a cathodic shift of ~150 mV on onset potential and a higher photocurrent density at lower bias can be observed in 6% $Co:BiVO_4$, which is quite similar as OECs modified $BiVO_4$ photoanodes. A photocurrent density of ~0.44 mA/cm^2 can be observed for 6% $Co:BiVO_4$ at 0.8 V vs RHE, whereas the value for pure $BiVO_4$ and 3% $Mo:BiVO_4$ is only 0.07 and 0.11 mA/cm^2 at the sample bias, respectively. However, with the further increase of applied bias, the photocurrent of $Co:BiVO_4$ increases quite slowly, and a photocurrent density of only 0.9 mA/cm^2 can be observed at 1.23 V vs RHE.

The J-V curves of $Mo:BiVO_4/Co:BiVO_4$ photoanodes with different Co doping concentrations were shown in Fig. 2b. The J-V curve of 2Mo-2Co-0% containing two layers of 3% $Mo:BiVO_4$ and two layers of pristine $BiVO_4$ is quite similar as that of $Mo:BiVO_4$, with an onset potential at ~0.5 V vs RHE and a photocurrent density of ~0.99 mA/cm^2 at 1.23 V vs RHE. The photocurrent of 2Mo-2Co-0% is slightly larger than that of $Mo:BiVO_4$, which could be due to the improved bulk charge separation efficiency by forming $Mo:BiVO_4/BiVO_4$ photoanodes. As Co^{2+} was doped into $BiVO_4$ layers, the photocurrent of $Mo:BiVO_4/Co:BiVO_4$ photoanodes can be greatly enhanced, which varied with the Co doping concentrations in $Co:BiVO_4$ layers. The photocurrent density initially increased with the increase of Co contents. And 2Mo-2Co-2% and 2Mo-2Co-4% yields a photocurrent density of 1.42 and 1.63 mA/cm^2 at 1.23 V vs RHE, respectively. 2Mo-2Co-6% yields the highest photocurrent density of about 1.98 mA/cm^2 at 1.23 V vs RHE, which is 200% and 220% as high as that of 2Mo-2Co-0% and 6% Co:BiVO4 with the same Co doping concentration, respectively. However, further increase on Co doping concentration would lead to a decrease on photocurrent, where 2Mo-2Co-8% yields a photocurrent density of 1.77 mA/cm^2 at 1.23 V vs RHE.

To be noticed, the onset potentials for the samples containing $Co:BiVO_4$ layers all lie at ~0.35 V vs RHE, which are ~150 mV lower than that of the samples without $Co:BiVO_4$ layers. This indicates the $Co:BiVO_4$ layers could act as OECs, which can lower the barriers for water oxidation and promote the interfacial charge separation during PEC water splitting. On the other hand, a built in electric field could be formed due to the variation on Fermi levels by Mo^{6+} and Co^{2+} doping, which could promote the charge separation during PEC water splitting as demonstrated in $W:BiVO_4/BiVO_4$ photoanodes reported recently [35]. Therefore, the enhanced photocurrents in $Mo:BiVO_4/Co:BiVO_4$ homojunctions photoanodes could be ascribed to the synergistic effects with both enhanced charge separation efficiencies in the bulk and at the interface.

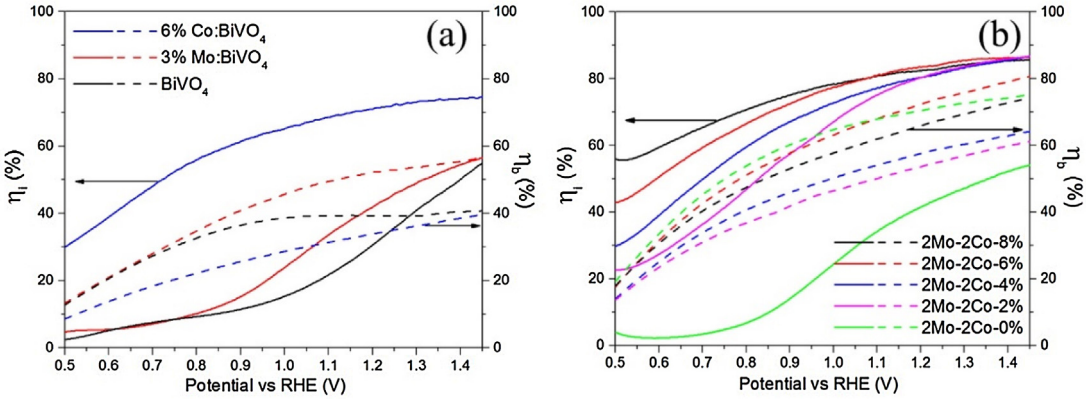

Fig. 3. Bulk and interfacial charge separation efficiencies of (a) $BiVO_4$, 3% Mo:$BiVO_4$ and 6% Co:$BiVO_4$ photoanodes, and (b) Mo:$BiVO_4$/Co:$BiVO_4$ homojunctions with different Co doping concentrations. The bulk (η_b) and interfacial charge separation efficiencies (η_i) was represented in dash and solid lines with the same color, respectively.

In order to verify the above assumption and further understand the mechanism for the enhanced PEC performances in Mo:$BiVO_4$/Co:$BiVO_4$ photoanodes, the charge separation efficiency both in the bulk (η_b) and at the electrode/electrolyte interface (η_i) of the above samples are further investigated. The details on the calculations of the charge separation efficiency in the bulk (η_b) and at the electrode/electrolyte interface (η_i) have been shown in Supporting Information. As shown in Fig. 3a, the charge separation efficiency of $BiVO_4$ is low either in the bulk or at the interface, with a η_b and η_i value of only 39.1% and 33.6% at 1.23 V vs RHE, respectively. The charge separation efficiency is slightly enhanced in Mo:$BiVO_4$, with a η_b and η_i value of 52.6% and 44.2% at 1.23 V vs RHE, respectively. This is accordant with the reported value, where the enhancement on charge separation efficiencies could be attributed to the improved electrical conductivity and reduced recombination due to the hexavalent Mo dopant as traps of photogenerated holes [10]. For Co:$BiVO_4$, a notable enhancement on interfacial charge separation efficiencies can be clearly observed as expected, with a η_i value of 71.7% at 1.23 V vs RHE, which is about 2.1 and 1.6 times of that for $BiVO_4$ and Mo:$BiVO_4$, respectively. This demonstrates Co:$BiVO_4$ could promote the interfacial charge separation during PEC water splitting similar as OECs, which can also explain the cathodic shift on onset potentials for the samples containing Co:$BiVO_4$ layers observed in Fig. 2. However, Co:$BiVO_4$ suffers from a poor bulk charge separation process with a η_i value of only 34.7%, which is even lower than that of $BiVO_4$.

Due to the catalytic activities of Co:$BiVO_4$ layers for water oxidation, the interfacial charge separation efficiencies in Mo:$BiVO_4$/Co:$BiVO_4$ photoanodes would also be improved with the assistance of Co:$BiVO_4$. As shown in Fig. 3b, 2Mo-2Co-0% without any Co ions yield a similar η_i value of 36.8% as pristine $BiVO_4$ at 1.23 V vs RHE. While, the introduction of only trace amount of Co ions could greatly enhance the interfacial charge separation efficiency. And the interfacial charge separation efficiencies of Mo:$BiVO_4$/Co:$BiVO_4$ photoanodes are directly dependent on the Co contents in Co:$BiVO_4$ layers, where the η_i values increase constantly with the increase of Co doping concentration. This can be easily understood that higher Co contents can provide more reactive sites during PEC water splitting, which result in higher charge separation efficiencies. However, with the increase of applied bias, the interfacial charge separation efficiencies of Mo:$BiVO_4$/Co:$BiVO_4$ are getting closer and reach a η_i value of ~80% at 1.23 V vs RHE. For comparison, Co-Pi modifed 3% Mo:$BiVO_4$ photoanode was also fabricated, and the interfacial charge separation efficiency has been ploted as shown in Fig. S6. At a bias of 1.23 V vs RHE, the η_i value for Co-Pi/Mo:$BiVO_4$ photoanode is calculated to be 82%, which is almost the same as Mo:$BiVO_4$/Co:$BiVO_4$ photoanodes, which confirmed that Co:$BiVO_4$ could play a simialr role as OECs, e.g., Co-Pi, during PEC water splitting.

For the bulk charge separation, a built in electric field would be formed at the interface between Mo:$BiVO_4$ and Co:$BiVO_4$ with different Co contents, which can provide a driven force to stimulate the charge separation. As shown in Fig. 3b, the η_b values for all these Mo:$BiVO_4$/Co:$BiVO_4$ photoanodes have been greatly enhanced. At the external bias of 1.23 V vs RHE, the η_b values for Mo:$BiVO_4$/Co:$BiVO_4$ photoanodes with Co doping concentration of 0%, 2%, 4%, 6% and 8% are 44.23%, 54.4%, 58.6%, 73.6% and 67.1%, respectively. 2Mo-2Co-6% yields the highest bulk charge separation efficiency of 73.6%, which has been enhanced by 88.2% and 39.9% compared with $BiVO_4$ and Mo:$BiVO_4$ photoanodes at the same bias, respectively. As the charge separation process is quite complex in Mo:$BiVO_4$/Co:$BiVO_4$ photoanodes, which typically involve three processes, namely, the charge transfer in Mo:$BiVO_4$ layers, across the Mo:$BiVO_4$/Co:$BiVO_4$ interface and in Co:$BiVO_4$ layers. The Mo:$BiVO_4$ layers in all Mo:$BiVO_4$/Co:$BiVO_4$ photoanodes are identical, therefore, the variation on η_b values in Mo:$BiVO_4$/Co:$BiVO_4$ photoanodes could be attributed to the differences on both the built in electric fields and the electrical properties in Co:$BiVO_4$ layers.

In order to further understand the bulk charge separation in Mo:$BiVO_4$/Co:$BiVO_4$ photoanodes with different Co contents, the electrical properties of Co:$BiVO_4$ layers with different Co contents and the built in electric fields in Mo:$BiVO_4$/Co:$BiVO_4$ photoanodes with different Co contents were further investigated. Mott-Schottky measurements were carried out to characterize the electrical properties of Co:$BiVO_4$ with different Co contents, which were performed at a frequency of 1 kHz in the dark as shown in Fig. 4a. All the samples exhibit a positive Mott-Schottky plots, which indicate they are n-type semiconductors. And the donor densities (N_d) of 3% Mo:$BiVO_4$, $BiVO_4$ and Co:$BiVO_4$ with Co contents of 2, 4, 6 and 8% were calculated by Mott-Schottky equation (see Supporting Information), with N_d values of 2.56×10^{20}, 4.16×10^{19}, 3.045×10^{19}, 2.225×10^{19}, 4.047×10^{19} and 1.48×10^{20} cm^{-3}, respectively. As expected, Mo^{6+} doping greatly increases the donor density in $BiVO_4$, where the N_d value of 3% Mo:$BiVO_4$ is nearly an order higher than that of pristine $BiVO_4$, which is consistent with the reported values. While, as Co^{2+} ions were doped into $BiVO_4$, the donor density decreased, which was quite different from Mo:$BiVO_4$. As $BiVO_4$ is an intrinsic n-type semiconductor, where oxygen vacancies were reported to be widely existed and responsible for the n-type conductivity of $BiVO_4$ [36]. When a small amount of Co^{2+} ions (2% and 4%) were doped into $BiVO_4$, the intrinsic oxygen vacancies (n-type defects) would be charge compensated by Co^{2+} (p-type dopants). As a result, the oxygen vacancies as well as the carrier concentrations in Co:$BiVO_4$

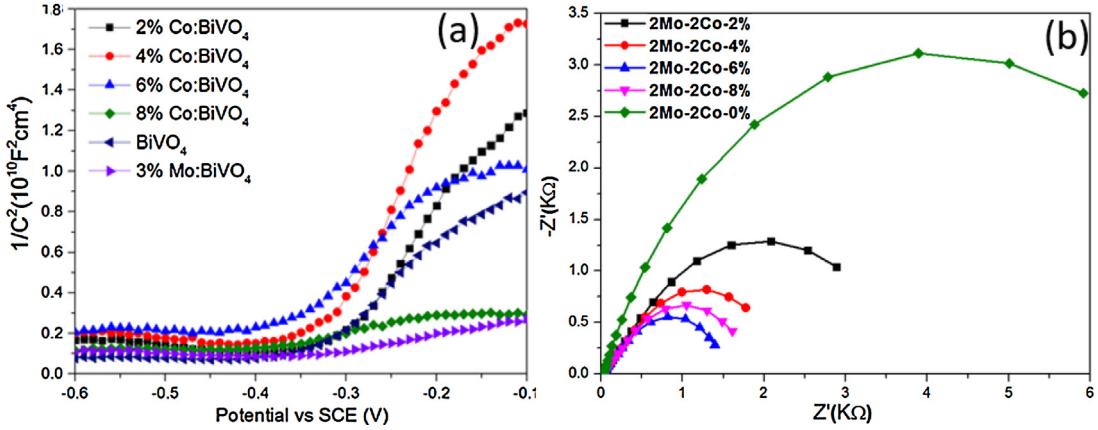

Fig. 4. (a) Mott-Schottky plots of $BiVO_4$, 3% Mo:$BiVO_4$ and Co:$BiVO_4$ with different Co contents measured at a frequency of 1 kHz in dark. (b) Nyquist plots of Mo:$BiVO_4$/Co:$BiVO_4$ homojunctions with different Co contents measured at 0 V vs SCE under light irradiation.

would be decreased. With the further increase of Co contents in Co:$BiVO_4$ (>6%), the formation energy of n-type defects would be lowered proportionally [20]. Therefore, new n-type defects (e.g., oxygen vacancies) would be formed again with the increasing the p-type dopants concentration, which subsequently increase the carrier density as well as the defect numbers in Co:$BiVO_4$ again as observed in 6% and 8% Co:$BiVO_4$. As discussed above, the carrier densities in Co:$BiVO_4$ are seem to be closely connected with the defect numbers, where the lower the donor density, the fewer the number of defects in Co:$BiVO_4$. However, they act oppositely during the charge separation process. Fewer defects would reduce the chance for carrier recombination during charge transfer, which are beneficial for the enhancement on bulk charge separation. While, lower donor densities would result in higher electrical resistances in Co:$BiVO_4$ layers, which would act negatively during charge transfer. Therefore, both of the carrier densities and the defect numbers in Co:$BiVO_4$ layers would affect the charge transfer during PEC water splitting.

The built in electric field in Mo:$BiVO_4$/Co:$BiVO_4$ photoanodes is another consideration for the bulk charge separation during PEC water splitting. However, it is quite difficult to be precisely measured or calculated owing to the more complex interfaces and surface states in the electrodes composed of nanomaterials. Therefore, the band bending (V_{bi}) and the intensity of the built in electric fields (E_{bi}) in Mo:$BiVO_4$/Co:$BiVO_4$ photoanodes with different Co contents were grossly estimated by using the equations for bulk semiconductor materials as follows: [35,37]

$$E_{bi} = \frac{2V_{bi}}{W}$$

$$V_{bi} = KT \ln \frac{N_{\text{Mo:BiVO4}}}{N_{\text{Co:BiVO4}}}$$

$$\mathrm{W} = \left(\frac{2\varepsilon\varepsilon_0}{e_0} \left(\frac{N_{\text{Mo:BiVO4}} + N_{\text{Co:BiVO4}}}{N_{\text{Mo:BiVO4}} N_{\text{Co:BiVO4}}} \right) \right)^{1/2}$$

where V_{bi} is the band bending at the Mo:$BiVO_4$/Co:$BiVO_4$ interface, W is the width of depletion region of the homojunction, k is the Boltzmann's constant, T is the temperature, e_0 is the electron charge, ε the relative permittivity of $BiVO_4$ ($\varepsilon = 68$) [38], ε the permittivity of vacuum and $N_{\text{Mo:BiVO4}}$ and $N_{\text{Co:BiVO4}}$ are the donor densities of Mo:$BiVO_4$ and Co:$BiVO_4$, respectively.

The band bending (V_{bi}), the widths of the depletion region (W) and the built in electric field intensities (E_{bi}) of the Mo:$BiVO_4$/Co:$BiVO_4$ photoanodes formed between 3% Mo:$BiVO_4$ and Co:$BiVO_4$ with different doping concentrations have been summarized in Table 1. The V_{bi} values formed between Mo:$BiVO_4$ and Co:$BiVO_4$ with different Co contents are reversely related to the donor densities of corresponding Co:$BiVO_4$ layers, where the homojunction consisted of 4% Co:$BiVO_4$ with the lowest donor density and 3% Mo:$BiVO_4$ yields the highest band bending of 0.063 eV. However, taking the width of depletion region into consideration, the Mo:$BiVO_4$/Co:$BiVO_4$ photoanodes consisted of 6% Co:$BiVO_4$ and 3% Mo:$BiVO_4$. However, the orders of neither V_{bi} nor E_{bi} in the homojunctions consisted of 3% Mo:$BiVO_4$ and Co:$BiVO_4$ with different Co contents are consistent with the order of η_b observed in Fig. 3b. This could also be an indicative that the bulk charge separation efficiency in Mo:$BiVO_4$/Co:$BiVO_4$ cannot be solely determined by the built in electric fields, but also closely related to the charge transfer in Co:$BiVO_4$ layers. With the synergistic effects of both the built in electric fields formed at the homojunction interface and the charge transfer in Co:$BiVO_4$ layers, the highest bulk charge separation efficiency can be obtained in the Mo:$BiVO_4$/Co:$BiVO_4$ photoanodes consisted of 3% Mo:$BiVO_4$ and Co:$BiVO_4$ with an optimum Co content of 6%.

Electrochemical Impendence Spectra (EIS) analysis is an effective way to reflect the charge separation properties during PEC water splitting. In order to further investigate the charge separation in Mo:$BiVO_4$/Co:$BiVO_4$ photoanodes, EIS analyses were carried out at 0 V vs SCE under light irradiation. Fig. 4b, shows the Nyquist plotes of Mo:$BiVO_4$/Co:$BiVO_4$ photoanodes containing two layers of 3% Mo:$BiVO_4$ and Co:$BiVO_4$ with different Co contents, respectively. The semicircle in the Nyquist plot at high frequencies is the characteristic of the charge transfer process, where the diameter of the semicircle is an indicative of the charge transfer resistance (R_{CT}) from the electrodes to electrolyte solutions. As can be observed in Fig. 4b, 2Mo-2Co-6% exhibits the smallest semicircle, with R_{CT} value of ~1.5 kΩ. And the 2Mo-2Co-8% exhibits the second smallest semicircle (with R_{CT} of ~1.8 kΩ). And the radii of the other Mo:$BiVO_4$/Co:$BiVO_4$ photoanodes constantly increase with the decrease of Co contents in Co:$BiVO_4$ layers, where the R_{CT} of 2Mo-2Co-4%, 2Mo-2Co-2% and 2Mo-2Co-0% is ~2.3 kΩ, ~3.8 kΩ and ~7.9 kΩ, respectively. That means the charge transfer from 2Mo-2Co-6% electrode to the electrolyte solution is much easier than in the other electrodes indicating the highest charge separation efficiency($\eta_b \times \eta_i$). And the charge separation efficiency in Mo:$BiVO_4$/Co:$BiVO_4$ photoanodes should follow the order: 2Mo-2Co-6% > 2Mo-2Co-8% > 2Mo-2Co-4% > 2Mo-2Co-2% > 2Mo-2Co-0%, which is consistent with the observation in the J-V curves in Fig. 2b and the charge separation efficiencies in Fig. 3b.

According to the above analysis, the charge transfer in Co:$BiVO_4$ layers is also an important consideration for bulk charge separation

Table 1
The calculated band bending (V_{bi}), the widths of depletion region (W) and electric field intensities (E_{bi}) of the homojunctions formed between 3% Mo:$BiVO_4$ and Co:$BiVO_4$ with different Co doping concentrations.

	$BiVO_4$ $N_d =$ $4.16 \times 10^{19} cm^{-3}$	2% Co:$BiVO_4$ $N_d =$ $3.045 \times 10^{19} cm^{-3}$	4% Co:$BiVO_4$ $N_d =$ $2.225 \times 10^{19} cm^{-3}$	6% Co:$BiVO_4$ $N_d =$ $4.047 \times 10^{19} cm^{-3}$	8% Co:$BiVO_4$ $N_d =$ $1.48 \times 10^{20} cm^{-3}$
3%Mo:Bi VO_4 $N_d = 2.56 \times 10^{20} cm^{-3}$	$V_{bi} = 0.047$ (eV) $W = 3.14$ (nm) $E_{bi} =$ 299 (KV/cm)	$V_{bi} = 0.055$ (eV) $W = 3.90$ (nm) $E_{bi} =$ 282 (KV/cm)	$V_{bi} = 0.063$ (eV) $W = 4.81$ (nm) $E_{bi} =$ 262 (KV/cm)	$V_{bi} = 0.048$ (eV) $W = 3.18$ (nm) $E_{bi} =$ 301 (KV/cm)	$V_{bi} = 0.014$ (eV) $W = 1.059$ (nm) $E_{bi} =$ 264 (KV/cm)

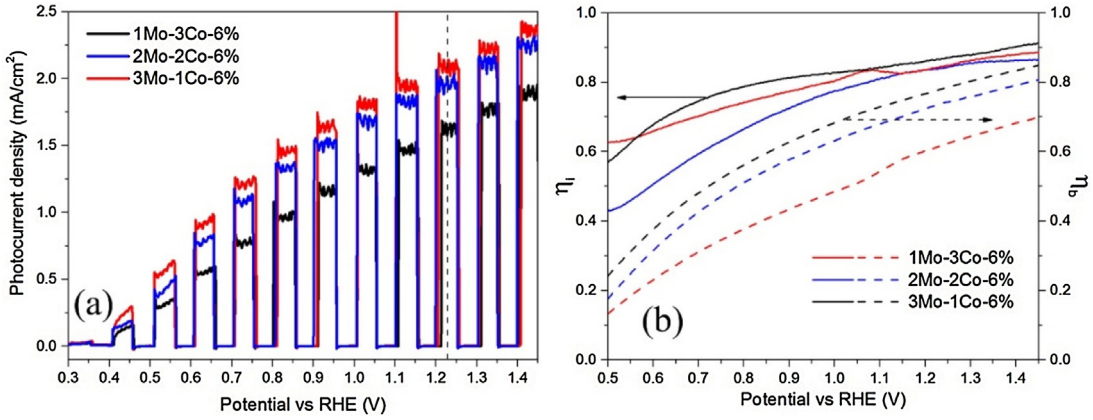

Fig. 5. (a) J-V curves and (b) Bulk and interfacial charge separation efficiencies of Mo:$BiVO_4$/Co:$BiVO_4$ photoanodes containing different layers of Co:$BiVO_4$.

in Mo:$BiVO_4$/Co:$BiVO_4$ photoanodes. Furthermore, only the surface of the Co:$BiVO_4$ layers are beneficial for the interfacial charge separation. Therefore, the charge separation efficiency and the PEC performance would be further improved by further decreasing the Co:$BiVO_4$ layer thicknesses. To demonstrate this assumption, 3Mo-1Co-6% consisted of three layers of 3% Mo:$BiVO_4$ and 1 layer Co:$BiVO_4$ with optimum Co content of 6% was fabricated. For comparison, 1Mo-3Co-6% containing 1 layer 3% Mo:$BiVO_4$ and 3 layers of 6% Co:$BiVO_4$ were also fabricated. As shown in the J-V curves in Fig. 5a, 3Mo-1Co-6% yields an enhanced photocurrent density of 2.09 mA/cm^2 at 1.23 V vs RHE as expected, which is 5% higher than that of 2Mo-2Co-6%. While, the photocurrent density of 1Mo-3Co-6% decreases to 1.63 mA/cm^2 at the same bias, which is only 82.3% of η_i that of 2Mo-2Co-6%. The bulk and interfacial charge separation efficiencies of Mo:$BiVO_4$/Co:$BiVO_4$ homojunctions containing different layers of Co:$BiVO_4$ were also plotted as shown in Fig. 5b. The interfacial charge separation efficiencies for the homojunctions containing different layers of Co:$BiVO_4$ are quite close with each other, which indicate only the Co ions on the surface of the electrode are useful for the interfacial charge separation. However, the bulk charge separation efficiencies can be effectively enhanced with the reduction of Co:$BiVO_4$ layers in the homojunctions, where the η_b value for 3Mo-1Co-6% and 1Mo-3Co-6% is 77.8% and 61.4%, respectively. That indicates the thickness of Co:$BiVO_4$ layers in Mo:$BiVO_4$/Co:$BiVO_4$ photoanodescan greatly influence the bulk charge separation during PEC water splitting. The stability of 3Mo-1Co-6% photoanode were also investigated in 0.1 M potassium phosphate aqueous solution at potential of 1.23 V vs RHE for 1 h. As shown in the *J-t* curve in Fig. S7a, the photocurrent slightly decreased from 2.09 to 1.52 mA/cm^2 during the experiment. This could be explained by the partial dissolution of the surface Co:$BiVO_4$ layer due to the chemical instability, which is quite similar as the prior reported results [39]. And gas bubbles can also be observed from the electrode, which were collected every 15 min and analyzed with gas chromatography. As shown in Fig. S7b, nearly stoichiometric H_2 and O_2 can be produced within experimental error.

Based on the above analyses, a plausible mechanism has been proposed to explain the improved PEC performances of Mo:$BiVO_4$/Co:$BiVO_4$ photoanodes as illustrated in Fig. 6. As n-type and p-type doping can shift the Fermi level of $BiVO_4$ towards the CBM and VBM, respectively. As Mo:$BiVO_4$ and Co:$BiVO_4$ were coupled together, a built-in electric field would be formed due to the opposite shift on Fermi levels by Mo^{6+} and Co^{2+} doping in $BiVO_4$, respectively. Because the Fermi level of Mo:$BiVO_4$ is very close to the CBM due to the n-type doping by Mo^{6+}, the built in electric field can be tuned by varying the Co^{2+} doping concentration. With the increase of Co contents in Co:$BiVO_4$ layers, the band bending at the Mo:$BiVO_4$/Co:$BiVO_4$ interface initially increases then decreased, where the homojunction consisted of 3% Mo:$BiVO_4$ and 4% Co:$BiVO_4$ exhibits the largest band bending of 0.063 eV. However, taking the width of depletion region into consideration, Mo:$BiVO_4$/Co:$BiVO_4$ photoanodes consisted of 3% Mo:$BiVO_4$ and 6% Co:$BiVO_4$ exhibit the largest E_{bi} value of 301 kV/cm. As the bulk charge separation involve the charge transfer in Mo:$BiVO_4$ layer, across the Mo:$BiVO_4$/Co:$BiVO_4$ interface and in Co:$BiVO_4$ layer, the bulk charge separation efficiency are not determined only by the built in electric fields formed between Mo:$BiVO_4$ and Co:$BiVO_4$, but also closely related to the charge transfer in Co:$BiVO_4$ layers. As electron acceptors, a trace amount of Co^{2+} can compensate the intrinsic defects in $BiVO_4$, which lower the carrier densities in Co:$BiVO_4$. However, as the Co^{2+} doping concentration is too high, more defects would be formed due to the self-compensation and increase the carrier densities. As the donor density and the defects act oppositely on the charge separation in Co:$BiVO_4$ layers, where lower donor density lead to larger resistance, while lower defect density reduce the charge recombination. With the synergistic effects of both the built-in electric field in the homojunctions and the electrical properties in Co:$BiVO_4$ layers, Mo:$BiVO_4$/Co:$BiVO_4$ photoanode consisted of 3% Mo:$BiVO_4$ and 6% Co:$BiVO_4$ exhibits

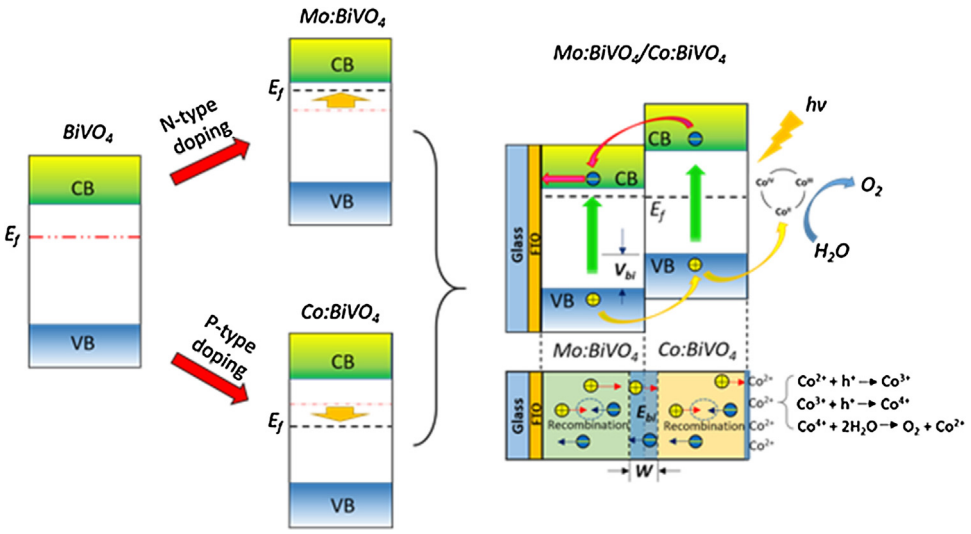

Fig. 6. Schematic illustration of the mechanism for the enhanced bulk and interfacial charge separation of Mo:$BiVO_4$/Co:$BiVO_4$ photoanodes.

the highest bulk charge separation efficiency. On the other hand, the Co:$BiVO_4$ layers on the surface of Mo:$BiVO_4$/Co:$BiVO_4$ photoanode are demonstrated to be able to act as reactive centers for water oxidation similar as Co-Pi, which can lower the onset potential for PEC water splitting and enhance the interfacial charge separation efficiencies. Our experimental results indicate the interfacial charge separation is closely related to the Co contents in Co:$BiVO_4$ layers, which can be explained by that high Co contents can provide more reactive sites for water oxidation leading to higher interfacial charge separation efficiencies. Based on the above analysis, Co:$BiVO_4$ layers in Mo:$BiVO_4$/Co:$BiVO_4$ photoanodes are regarded as the most important issue for the enhanced PEC performances, which can not only promote the interfacial charge separation due to its catalytic property, but also be able to promote the bulk charge separation by tuning the built in electric fields of the homojunction and the charge transfer in Co:$BiVO_4$ layers by varying the Co contents. As a result, both the bulk and interfacial charge separation efficiency in Mo:$BiVO_4$/Co:$BiVO_4$ photoanodes can be greatly improved, which lead to enhanced PEC water splitting performances. With the further optimization of the layer numbers of Mo:$BiVO_4$ and Co:$BiVO_4$ layers in Mo:$BiVO_4$/Co:$BiVO_4$ photoanodes and the synergistic consideration of both bulk and interfacial charge separation efficiencies, 3Mo-1Co-6% consisted of 3 layers of Mo:$BiVO_4$ and 1 thin layer of 6% Co:$BiVO_4$ exhibited the highest charge separation efficiencies and the best PEC performances during PEC water splitting.

In conclusion, we fabricated Mo:$BiVO_4$/Co:$BiVO_4$ photoanodes by depositing Co:$BiVO_4$ layers on top of Mo:$BiVO_4$ layers, and demonstrated the enhanced PEC performances with improved charge separation both in the bulk and at the interface by doping strategy. According to our experimental results, the Co:$BiVO_4$ layers in Mo:$BiVO_4$/Co:$BiVO_4$ photoanodes are found to be important for the enhanced PEC performances, where the Co^{2+} ions on the surface can act as reactive centers for water oxidation to promote the interfacial charge separation, while, the Co^{2+} doping in $BiVO_4$ cannot only tune the built in electric fields in the electrodes, but also be able to affect the charge transfer in Co:$BiVO_4$ layers, which acted synergistically to influence the bulk charge separation. With the assistance of Co:$BiVO_4$ layers, both the bulk and interfacial charge separation efficiencies can be effectively enhanced in Mo:$BiVO_4$/Co:$BiVO_4$ photoanodes even without the modification of any OECs, which lead to enhanced PEC performances. By varying the Co contents and the layer numbers of Co:$BiVO_4$ in Mo:$BiVO_4$/Co:$BiVO_4$ photoanodes, the optimized PEC performances can be observed in 3Mo-1Co-6% consisted of 3 layers of 3% Mo:$BiVO_4$ and 1 layer of 6% Co:$BiVO_4$, which yields a photocurrent density of 2.09 mA/cm^2 at 1.23 vs RHE, with a η_b and η_i value of 77.8% and 86.5%, respectively. This work may provide a new method for the design and fabrication of high efficient photoanodes by doping strategy with high bulk and interfacial charge separation efficiencies, which could be useful for the further development and practical applications of PEC water splitting.

Acknowledgements

This work is financially supported by the National Basic Research Program of China (the 973 program, 2013CB632401), the National Natural Science Foundation of China (21333006, 21573135, 11374190, 51602179 and 51321091), and the Shandong Provincial Natural Science Foundation (ZR2014BM024). B.B.H. acknowledges support from the Taishan Scholars Program of Shandong Province, and Z.Y.W. acknowledges support from Young Scholars Program (2015WLJH35) and Fundamental Research Funds of Shandong University (2014JC049).

Appendix A. Supplementary data

Supplementary data associated with this article can be found, in the online version, at http://dx.doi.org/10.1016/j.apcatb.2017.03.078.

References

[1] T. Bak, J. Nowotny, M. Rekas, C.C. Sorrell, Int. J. Hydrogen Energy 27 (2002) 991–1022.
[2] J.Z. Zhang, MRS Bull. 36 (2011) 48–55.
[3] Shahed U.M. Khan, Mofareh Al-Shahry, William B. Ingler, Science 297 (2002) 2243–2245.
[4] B. Zhang, Z.Y. Wang, B.B. Huang, X.Y. Zhang, X.Y. Qin, H.L. Li, Y. Dai, Y.J. Li, Chem. Mater. 28 (2016) 6613–6620.
[5] T.W. Kim, K.-S. Choi, Science 343 (2014) 990–994.
[6] D.K. Zhong, M. Cornuz, K. Sivula, M. Grätzel, D.R. Gamelin, Energy Environ. Sci. 4 (2011) 1759–1764.
[7] R. Abe, M. Higashi, K. Domen, J. Am. Chem. Soc. 132 (2010) 11828–11829.
[8] Y.B. Li, T. Takata, D. Cha, K. Takanabe, T. Minegishi, J. Kubota, K. Domen, Adv. Mater. 25 (2013) 125–131.
[9] A. Kudo, K. Omori, H. Kato, J. Am. Chem. Soc. 121 (1999) 11459–11467.
[10] H.W. Jeong, T.H. Jeon, J.S. Jang, W. Choi, H. Park, J. Phys. Chem. C 117 (2013) 9104–9112.
[11] Z.Y. Jiang, Y.Y. Liu, T. Jing, B.B. Huang, X.Y. Zhang, X.Y. Qin, Y. Dai, M.-H. Whangbo, J. Phys. Chem. C 120 (2016) 2058–2063.
[12] J.Z. Su, L.J. Guo, N.Z. Bao, C.A. Grimes, Nano Lett. 11 (2011) 1928–1933.

[13] M.Z. Xie, X.D. Fu, L.Q. Jing, P. Luan, Y.J. Feng, H.G. Fu, L. Lived, Adv. Energy Mater. 4 (2014) 1300995.
[14] D.K. Zhong, S.J. Choi, D.R. Gamelin, J. Am. Chem. Soc. 133 (2011) 18370–18377.
[15] Y. Liu, Y.H. Guo, L.T. Schelhas, M. Li, J.W. Ager, J. Phys. Chem. C 120 (2016) 23449–23457.
[16] S.J.A. Moniz, J. Zhu, J. Tang, Adv. Energy Mater. 4 (2014) 1301590.
[17] M. Zhong, T. Hisatomi, Y. Kuang, J. Zhao, M. Liu, A. Iwase, Q.M. Jia, H. Nishiyama, T. Minegishi, M. Nakabayashi, N. Shibata, R. Niishiro, C. Katayama, H. Shibano, M. Katayama, A. Kudo, T. Yamada, K. Domen, J. Am. Chem. Soc. 137 (2015) 5053.
[18] H. Ye, J. Lee, J.S. Jang, A.J. Bard, J. Phys. Chem. C 114 (2010) 13322–13328.
[19] H. Ye, H.S. Park, A.J. Bard, J. Phys. Chem. C 115 (2011) 12464–12470.
[20] J.Z. Zhang, K.F. Tse, M.H. Wong, Y. Zhang, J.Y. Zhu, Front. Phys. 11 (2016) 117405.
[21] B.S. Brunschwig, M.H. Chou, C. Creutz, P. Ghosh, N. Sutin, J. Am. Chem. Soc. 105 (1983) 4832–4833.
[22] T. Schmidt, H. Wendt, Acta 39 (1994) 1763–1767.
[23] Y. Matsumoto, E. Sato, Mater. Chem. Phys. 14 (1986) 397–426.
[24] W.K. Behl, J.E. Toni, J. Electroanal. Chem. 31 (1971) 63–75.
[25] G.L. Elizarova, G.M. Zhidomirov, V.N. Parmon, Catal. Today 58 (2000) 71–88.
[26] A. Kay, I. Cesar, M. Grätzel, J. Am. Chem. Soc. 128 (2006) 15714–15721.
[27] L. Chen, F.M. Toma, J.K. Cooper, A. Lyon, Y. Lin, I.D. Sharp, J.W. Ager, ChemSusChem 8 (2015) 1066–1071.
[28] Y.C. Qiu, W. Liu, W. Chen, W. Chen, G.M. Zhou, P.-C. Hsu, R.F. Zhang, Z. Liang, S.S. Fan, Y.G. Zhang, Y. Cui, Sci. Adv. 2 (2016) e1501764.
[29] H.W. Jeong, T.H. Jeon, J.S. Jang, W. Choi, H. Park, J. Phys. Chem. C 117 (2013) 9104–9112.
[30] S.M. Thalluri, S. Hernández, S. Bensaid, G. Saracco, N. Russo, Appl. Catal. B: Environ. 180 (2016) 630–636.
[31] S.K. Pilli, T.E. Furtak, L.D. Brown, T.G. Deutsch, J.A. Turner, A.M. Herring, Energy Environ. Sci. 4 (2011) 5028–5034.
[32] A. Lu, Y.Z. Chen, J.R. Jin, G.-H. Yue, D.-L. Peng, J. Power Sources 220 (2012) 391–398.
[33] C.R. Brundle, T.J. Chuang, D.W. Rice, Surf. Sci. 60 (1976) 286–300.
[34] W.J. Luo, J.J. Wang, X. Zhao, Z.Y. Zhao, Z.S. Li, Z.G. Zou, Phys. Chem. Chem. Phys. 15 (2013) 1006.
[35] F.F. Abdi, L.H. Han, A.H.M. Smets, M. Zeman, B. Dam, Roel van de Krol1, Nat. Commun. 4 (2013) 2195.
[36] J.K. Cooper, S.B. Scott, Y. Ling, J.H. Yang, S.J. Hao, Y. Li, F.M. Toma, M. Stutzmann, K.V. Lakshmi, Ian D. Sharp, Chem. Mater. 28 (2016) 5761–5771.
[37] S.M. Sze, Physics of Semiconductor Devices, Murray Hill, New Jersey, USA, 1981.
[38] D. Zhou, L.X. Pang, J. Guo, Z.M. Qi, T. Shao, Q.P. Wang, H.D. Xie, X.Y. Clive, A. Randall, Inorg. Chem. 53 (2014) 1048–1055.
[39] T.W. Kim, K.-S. Choi, J. Phys. Chem. Lett. 7 (2016) 447–451.